

# Shape, Mean Radius, Gravity Field, and Interior Structure of Callisto

J. D. Anderson, R. A. Jacobson, and T. P. McElrath

*Jet Propulsion Laboratory, California Institute of Technology, 4800 Oak Grove Drive, MS 238-420, Pasadena, California 91109-8099*  
E-mail: john.d.anderson@jpl.nasa.gov

W. B. Moore and G. Schubert

*Department of Earth and Space Sciences, Institute of Geophysics and Planetary Physics, University of California, Los Angeles, California 90095-1567*

and

P. C. Thomas

*Cornell University, Center for Radiophysics and Space Research, 422 Space Science Building, Ithaca, New York 14853-6801*

Received March 27, 2000; revised April 23, 2001

**Radio Doppler data generated by the Deep Space Network (DSN) from five encounters of the Galileo spacecraft with Callisto, Jupiter's outermost Galilean satellite, have been used to determine the mass (GM) and unnormalized quadrupole gravity coefficients in Callisto's external gravitational field. The results are  $GM = (7179.292 \pm 0.009) \text{ km}^3 \text{ s}^{-2}$ ,  $J_2 = (32.7 \pm 0.8) \times 10^{-6}$ ,  $C_{22} = (10.2 \pm 0.3) \times 10^{-6}$ ,  $S_{22} = (-1.1 \pm 0.3) \times 10^{-6}$ ,  $C_{21} = (0.0 \pm 0.3) \times 10^{-6}$ , and  $S_{21} = (0.0 \pm 1.6) \times 10^{-6}$ . Also, four spacecraft images of Callisto have been used to determine its mean radius. The result is  $R = (2410.3 \pm 1.5) \text{ km}$ , with no detectable deviation from sphericity. Derived parameters are Callisto's mean density of  $(1834.4 \pm 3.4) \text{ kg m}^{-3}$  and axial moment of inertia  $C/MR^2 = 0.3549 \pm 0.0042$ . While the mean density indicates that Callisto is a mixture of rock and ice, the moment of inertia is too small for a homogeneous mixture. Accordingly, we present a suite of possible two- and three-layer interior models that satisfy the given constraints for radius, density, and moment of inertia. While not unique, these models show that Callisto cannot be entirely differentiated, and that there must exist a region of mixed ice and rock-metal, possibly extending to the center of the satellite.** © 2001 Academic Press

## 1. INTRODUCTION

After the exploration of the Jupiter system during the Galileo spacecraft's first 11 orbital revolutions of Jupiter, a follow-on Galileo Europa mission (GEM) focused on the exploration of Europa during orbital revolutions 12 to 19. We reported gravity and interior results for Europa from four encounters on orbital revolutions 4, 6, 11, and 12 (Anderson *et al.* 1998a). Additional GEM encounters confirmed that the published Europa gravity field is correct (Jacobson *et al.* 1999). On the other hand, pre-

viously reported results for Callisto, from orbital revolutions 3, 9, and 10 (Anderson *et al.* 1997, Anderson *et al.* 1998b), left some ambiguities about whether the rock and ice within Callisto are separated partially or not at all, the only definite conclusion being that a complete separation is ruled out.

Here we use additional radio Doppler data from close encounters with Callisto during a perijove reduction campaign on orbital revolutions 20 to 23, a campaign carried out to facilitate close encounters with Io on orbital revolutions 24 and 25. Of the four available GEM Callisto encounters, it is the one on the 21st orbital revolution (C21) that yields most of the new gravity information. Although we have fit Doppler data for five encounters separately and in combination, it is essentially the data on the 10th and 21st orbital revolutions (C10 and C21) that determine Callisto's gravity field. In addition, four good images of Callisto's limb, taken with the Galileo imaging system, yield new results for the satellite's shape and mean radius. These new data on shape and gravity field provide important constraints on possible Callisto interior models.

## 2. SHAPE AND MEAN RADIUS

The technique of using spacecraft imaging data to determine the shape of a satellite has been discussed before in detail (Dermott and Thomas 1988, 1994, Thomas *et al.* 1998). The technique measures limb positions by matching a model of a bright edge and spread function to the observed brightness scanned off the limb. The image coordinates are corrected to coordinates in kilometers at the target satellite by means of navigation data for the spacecraft position, and camera focal length and distortion (Davies *et al.* 1994). With the inclusion of an adjustment for camera pointing, the ellipsoidal shape can be

**TABLE I**  
**Fits of Triaxial Ellipsoid Models to Imaging Limb Data**

Image number <sup>a</sup>	N <sup>b</sup>	Equilibrium <sup>c</sup>	Best fit <sup>d</sup>	km/pixel	Latitude <sup>e</sup>	Longitude <sup>e</sup>
383944100	293	0.096	0.096	9.48	1.91	28.64
389556200	605	0.169	0.170	6.47	-0.17	65.86
420426068	387	0.089	0.090	13.96	-0.47	56.27
420426101	479	0.117	0.117	13.96	-0.47	56.26

<sup>a</sup> Galileo image number from Planetary Data System (PDS) catalog.

<sup>b</sup> Number of data points on the limb for each image.

<sup>c</sup> RMS residual (pixels) with equilibrium fitting model, a = 2410.4 km, b = 2410.3 km, c = 2410.3 km.

<sup>d</sup> RMS residual (pixels) with ellipsoidal fitting model, a = 2410.4 km, b = 2410.2 km, c = 2410.3 km.

<sup>e</sup> Latitude and west longitude (deg) of the sub-spacecraft point in Callisto-fixed IAU coordinate system (Davies *et al.* 1996).

determined by matching the limb coordinates to those predicted for triaxial ellipsoids. We solve for the shape in two ways. First, we determine the best ellipsoid with no constraints on shape, then we determine a shape with the relative axial dimensions constrained by equilibrium theory (Dermott and Thomas 1988, 1994). Because only a few Galileo images of Callisto covered a large fraction of the limb, the accuracy of both solutions for Callisto's shape is limited.

The results of fitting two ellipsoidal shapes to the imaging data are given in Table I. Both solutions produce a nearly spherical shape, and in fact any difference between them is not statistically significant. Both fits, with RMS residuals well under 0.2 pixels, indicate little global departure from sphericity. The uncertainty in the relative measures (such as a-c) can be evaluated formally by a chi-square method (Dermott and Thomas 1988, 1994), but because this method ignores the systematic error, the resulting formal errors are not realistic. Instead, we estimate the realistic errors by noting that the range of solutions for a-c from individual profiles is 0.6 km and that the systematic error for the differences in the axes should be no more than twice this range, still less than 0.2 pixels. However, because of the use of summed pixel images, the absolute calibration of the limb location can be even less accurate (Thomas *et al.* 1998). Therefore, we adopt a realistic uncertainty in the mean radius of 1.5 km, 25% larger than twice the range of all solutions for the difference in axes. The final result is a mean radius  $R = 2410.3 \text{ km} \pm 1.5 \text{ km}$ , with no detectable deviation from sphericity. All three principal axes are equal to  $R$  with a realistic error (random and systematic) of  $\pm 1.5 \text{ km}$ .

### 3. GRAVITY FIELD

The geometry of the Callisto encounters used in the gravity analysis has been discussed before (Anderson *et al.* 1998b, Jacobson *et al.* 1999). For the two best gravity encounters, C10 occurred at an altitude of 528 km, a latitude of  $4.6^\circ$ , and a longitude of  $78.7^\circ \text{ W}$ , while C21 occurred at an altitude of 1041 km, a

latitude of  $-0.7^\circ$ , and a longitude of  $286^\circ \text{ W}$ , where altitude is referred to a sphere of radius 2410.3 km, and latitude and longitude are defined by international convention (Davies *et al.* 1996). The Earth-spacecraft line of sight was  $90^\circ$  from the Callisto-centered trajectory for C10 and  $32^\circ$  for C21. Consequently, our previous concern (Anderson *et al.* 1998b) that the gravity perturbations are only measurable perpendicular to the C10 trajectory (cross track) has been alleviated by measurements of both along-track and cross-track components for C21. These two components are in the trajectory plane, unlike the third normal component which yields negligible gravity information.

For purposes of modeling the gravity field, we use the standard Legendre expansion of the potential function  $V$  in spherical harmonics (Kaula 1966).

$$V(r, \phi, \lambda) = \frac{GM}{r} \left[ 1 + \sum_{n=2}^{\infty} \sum_{m=0}^n \left( \frac{R}{r} \right)^n (C_{nm} \cos m\lambda + S_{nm} \sin m\lambda) P_{nm}(\sin \phi) \right], \quad (1)$$

where  $M$  is the satellite's mass, and  $G$  is the gravitational constant;  $G = (6.67259 \pm 0.00085) \times 10^{-11} \text{ m}^3 \text{ kg}^{-1} \text{ s}^{-2}$  (Cohen and Taylor 1999). The spherical coordinates  $(r, \phi, \lambda)$  are referred to the center of mass, with  $r$  the radial distance,  $\phi$  the latitude, and  $\lambda$  the longitude on the equator. Callisto's mean radius  $R$  from Section 2 is  $2410.3 \pm 1.5 \text{ km}$ ;  $P_{nm}$  is the associated Legendre polynomial of degree  $n$  and order  $m$ ; and  $C_{nm}$  and  $S_{nm}$  are the corresponding harmonic coefficients. We limit the Callisto gravity parameters to the monopole  $GM$  and to the five quadrupole coefficients  $J_2$  ( $-C_{20}$ ),  $C_{21}$ ,  $S_{21}$ ,  $C_{22}$ , and  $S_{22}$ . These coefficients, along with other parameters in the fitting model, are determined from the data by weighted least squares (Moyer 1971, Tapley 1973, Anderson 1974, Lawson and Hanson 1974). All other gravity harmonics are set to zero by default. Of course all other harmonics are not exactly zero, but the data can be fit to the noise level with just  $GM$  and the quadrupole moments, hence there is no point in including more coefficients. More coefficients would just make the solution ill conditioned and would require the inclusion of a priori information on the gravity field or, alternatively, the use of singular value decomposition (SVD) (Lawson and Hanson 1974). Basically, the flyby distances are not close enough for a detection of gravity moments beyond the quadrupole terms.

As in previous analyses (Anderson *et al.* 1998a, Anderson *et al.* 1998b), the gravity coefficients are determined by analyzing each encounter separately and also in combination. As might be expected, there is not enough information from a single encounter to determine all five quadrupole coefficients, and although the separate determinations are useful for running consistency checks, they yield little substantive information. Therefore, we present here just the results from our best combined fit (JUP158), with details of the methodology presented elsewhere (Anderson *et al.* 1998b, Jacobson *et al.* 1999). The

Callisto encounters included in the fit are C3, C9, C10, C20, and C21. The fit JUP158 yields  $GM = 7179.292 \pm 0.009 \text{ km}^3 \text{ s}^{-2}$ , and the quadrupole coefficients are  $J_2 = (32.7 \pm 0.8) \times 10^{-6}$ ,  $C_{22} = (10.2 \pm 0.3) \times 10^{-6}$ ,  $S_{22} = (-1.1 \pm 0.3) \times 10^{-6}$ ,  $C_{21} = (0.0 \pm 0.3) \times 10^{-6}$ , and  $S_{21} = (0.0 \pm 1.6) \times 10^{-6}$ . The correlation coefficient between  $J_2$  and  $C_{22}$  is 0.997, a reflection of the near equatorial nature of all the encounters. The quoted errors represent our best estimates of the realistic errors.

#### 4. INTERPRETATION

As pointed out previously (Anderson *et al.* 1997), it is unlikely that the rigidity of materials that make up Callisto could hide a strongly differentiated satellite. Therefore, we employ equilibrium theory (Hubbard and Anderson 1978, Mueller and McKinnon 1988, Zharkov *et al.* 1985, Schubert *et al.* 1994) in all the interpretations of results, and we take  $C_{22}$  and the mean density as the sole gravitational constraints on interior models. The values of  $GM$  and  $R$  inferred from the Galileo Doppler and imaging data yield a mean density of  $1834.4 \pm 3.4 \text{ kg m}^{-3}$  for Callisto, where the density error is dominated by the  $\pm 1.5 \text{ km}$  error in the mean radius  $R$ .

Under the assumption that Callisto's spherical harmonic degree 2 gravitational field is due to the equilibrium tidal and rotational ellipsoidal distortion of a satellite in synchronous rotation with its orbital period, the gravity coefficient  $C_{22}$  is related to the rotational parameter  $q_r$  by

$$C_{22} = \frac{3\alpha q_r}{4}, \quad (2)$$

where  $q_r = \omega^2 R^3 / GM$  is a measure of the forcing for rotational flattening of the satellite. The rotational angular velocity  $\omega$  is equal to Callisto's orbital angular velocity of  $21.5711 \text{ deg day}^{-1}$  (Greenberg 1982), and  $q_r$  is  $37.034 \pm 0.069$  in units  $10^{-6}$ . The dimensionless response coefficient  $\alpha$  depends on the distribution of density with depth inside the satellite ( $\alpha = 0.5$  for constant density). For our adopted value of  $C_{22}$ ,  $\alpha$  is  $0.371 \pm 0.011$ . From equilibrium theory and the value of  $\alpha$ , it follows that Callisto's axial moment of inertia  $C$ , normalized to  $MR^2$ , is  $C/MR^2 = 0.3549 \pm 0.0042$ , as computed from the approximate Radau relationship (Hubbard and Anderson 1978),

$$\frac{C}{MR^2} = \frac{2}{3} \left[ 1 - \frac{2}{5} \left( \frac{4 - 3\alpha}{1 + 3\alpha} \right)^{1/2} \right]. \quad (3)$$

Similarly, the differences in Callisto's principal axes ( $c < b < a$ ) can be computed from (Hubbard and Anderson 1978)

$$\frac{a - c}{c} = 2q_r(1 + 3\alpha), \quad (4)$$

where  $c$  is the polar radius and  $(b - c)/(a - c)$  is exactly  $1/4$ . The difference in axes as inferred from the gravity field is  $a - c = (377.2 \pm 5.9) \text{ m}$ ,  $b - c = (94.3 \pm 1.5) \text{ m}$ , and  $a - b = (282.9 \pm$

$4.4) \text{ m}$ , which is consistent with the measured shape from Section 2, where  $a - c = (0.1 \pm 1.2) \text{ km}$ , including both random and systematic error. We ignore the small differences between the three axes, and hence the three principal moments, and use the normalized axial moment of inertia and the mean density to interpret results. Our determination of  $J_2$  yields a value for  $\alpha$  that is just barely consistent at the one sigma level with our adopted value from  $C_{22}$ . If there were a Callisto encounter at high latitude, this would be of concern, but with only equatorial flybys, it is not statistically significant.

The inferred value of  $C/MR^2$  is significantly less than 0.4, the value of  $C/MR^2$  for a sphere of constant density, and is also less than the value of 0.38 for an undifferentiated model of Callisto including ice phase changes (McKinnon 1998). There must be an increase in rock-metal fraction with depth inside Callisto, and consequently Callisto must be at least partially differentiated.

Consistent with the few constraints we have on Callisto's internal structure (mean density and moment of inertia), we explore simple two- and three-layer models of its interior density. We use a forward modeling approach and solve Clairaut's equation for the distortion of a satellite with a given internal structure. Even the simple parameterizations adopted here are underconstrained, so we present families of possible hydrostatic internal structures consistent with the observed mean density and  $C_{22}$ .

The two free parameters of the two-layer models shown in Fig. 1 are the densities of the layers. The interior density ranges from the mean density of Callisto to the density of iron. The outer shell density ranges from the density of ice to less than the mean density of Callisto. The thin solid lines in the figure give the thickness of the outer layer in kilometers. The thick solid curve is the locus of all two-layer models with the observed value of  $C_{22}$ . The thick dashed lines show the limits on the models based on the  $\pm 1\sigma$  values of  $C_{22}$ . Models which have the observed value of  $C_{22}$  fall between two end members: a relatively pure ice outer shell about 300 km thick overlying a mixed ice and rock-metal

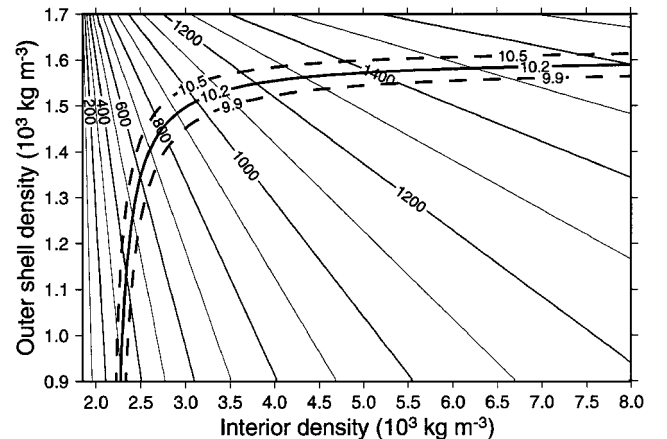


**FIG. 1.** Two-layer models of Callisto's interior density consistent with the observed mass and moment of inertia. Bold curves give the family of models for the nominal (solid) and one-sigma (dashed) values of  $C_{22}$ . Thin lines are labeled by the thickness of the outer shell in km.

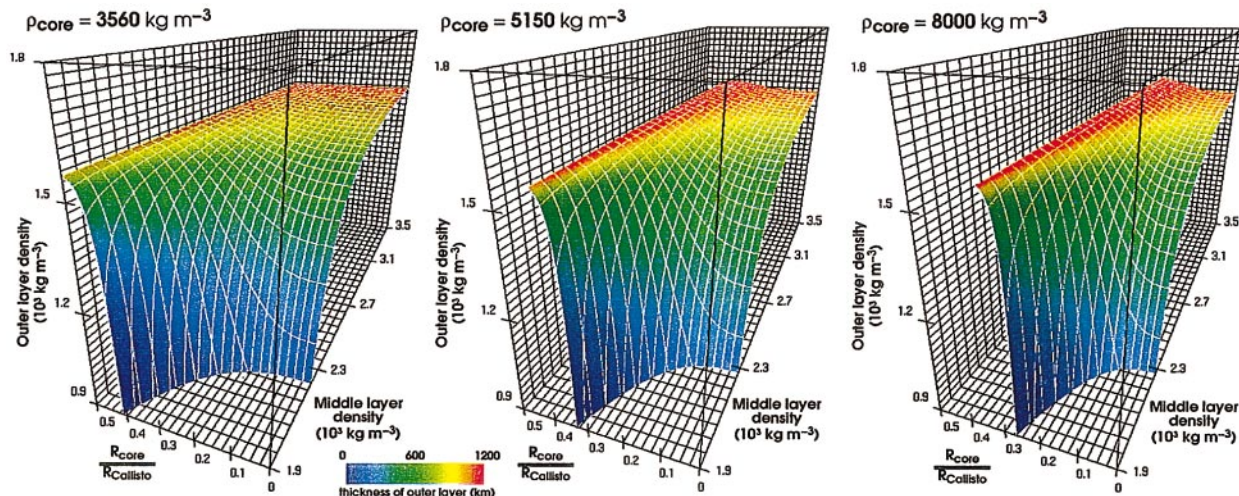


**FIG. 2.** Three-layer models of Callisto's interior density consistent with the observed mass and moment of inertia for core densities equal to (left to right) bulk Io ( $3560 \text{ kg m}^{-3}$ ), an Fe–FeS eutectic ( $5150 \text{ kg m}^{-3}$ ), and pure iron ( $8000 \text{ kg m}^{-3}$ ). The surface in three-dimensional parameter space is the family of solutions that fit the observed constraints. The color of the surface gives the thickness of the outer layer as indicated by the colorbar.

interior of density near  $2300 \text{ kg m}^{-3}$ , and a thick (greater than about  $1000 \text{ km}$ ) ice and rock–metal outer shell with a density near  $1600 \text{ kg m}^{-3}$  overlying a rock–metal core.

The two-layer models are a subset ( $R_{\text{core}}/R_{\text{Callisto}} = 0$ ) of the three-layer models shown in Fig. 2 for core densities corresponding to the mean density of Io ( $3560 \text{ kg m}^{-3}$ ), the density of Fe–FeS ( $5150 \text{ kg m}^{-3}$ ), and the density of Fe ( $8000 \text{ kg m}^{-3}$ ). Models that satisfy the mean density and moment of inertia constraints are defined by the surfaces in the three-dimensional parameter space consisting of normalized core radius, middle layer density, and outer layer density. While a wide range of internal density models is consistent with the observations of Callisto's mean density and moment of inertia, it is possible to reach a number of robust conclusions about Callisto's interior.

Figure 3 shows the families of three-layer models for which the outer shell has a density appropriate for clean ice ( $1000 \text{ kg m}^{-3}$ ). Solid lines are for the nominal value of  $C_{22}$

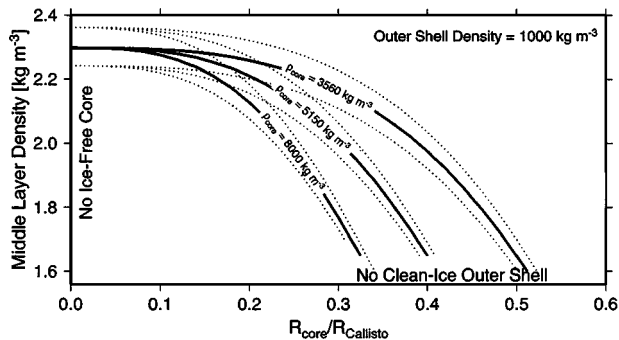


**FIG. 3.** Three-layer models with outer shell density =  $1000 \text{ kg m}^{-3}$ . The curves give the family of models for the nominal (solid) and one-sigma (dotted) values of  $C_{22}$ . The lines are labeled by the density of the core.

and dotted lines represent the one-sigma variations. The curves are labeled according to the density of the core. These models are bracketed by the end-member two-layer models of Fig. 1. In between the extremes are several similar families of models with middle layer densities between  $1600$  and  $2300 \text{ kg m}^{-3}$ . In every case, a significant portion of Callisto has a density that can only be explained by a mixture of ice and rock or rock–metal. Thus, Callisto must only be partially differentiated, with the ice and rock incompletely separated. The rock–metal fraction in Callisto must increase with depth, but gravity data are unable to constrain the exact nature of the increase (either continuous or step-wise). Whatever the distribution of rock–metal fraction with depth, it is certain that ice and rock–metal are mixed together to depths of at least about  $1000 \text{ km}$  and even, perhaps, to the center of the satellite.

Based on arguments that subsolidus ice convection is necessary to remove the radiogenically generated heat from the rocks in Callisto's interior, and that such thermal convection would be inhibited by negative compositional buoyancy if rock–metal fraction increased gradually with depth, we prefer either a two-layer model in which a large ice–rock–metal core of essentially uniform composition is surrounded by a relatively clean ice shell up to about  $350 \text{ km}$  thick, or a similar three-layer model which also has an inner rock–metal core. However, it is difficult to reconcile a metallic core with the requirement that ice and rock remain mixed throughout large portions of the interior. Separation of rock and metal requires temperatures far in excess of the melting point of ice, so formation of a metallic core in Callisto should also imply complete separation of ice and rock. Formation of a rock core is less problematic, although even in this case, the consolidation of a large (40% Callisto's radius) rock core could release enough energy to melt a large fraction (50%) of Callisto's ice, resulting in complete separation of ice

and rock. It is therefore considered unlikely that a rock core of radius larger than about 25% of Callisto's radius exists at the center of the satellite.

Since ice and rock–metal are mixed together to great depth in Callisto, ice–rock differentiation must be a slow process in the satellite. It cannot involve substantial melting of ice for then there would be rapid separation of the rock–metal and water components; it must be a sluggish, subsolidus process. Rock–metal should eventually sink through the ice to the center of Callisto but the rate at which this occurs will depend on the size of the rock–metal particles, their density, the viscosity of the ice, and the vigor of convection in the ice. Ice–rock differentiation may have cleaned a relatively thin shell near the surface of Callisto, but the process has not proceeded to completion. Ice–rock differentiation must be an ongoing process.

If a satellite as ice-rich as Callisto is capable of maintaining elastic stresses over geologic time, then the assumption of a hydrostatic figure would be incorrect and Callisto's moment of inertia could be smaller than we inferred from  $C_{22}$  using the equilibrium assumption. The amount of ice–rock separation we report is a lower limit and Callisto could be hiding a more differentiated interior beneath a strong elastic shell.

Incomplete separation of ice and rock in Callisto is consistent with other observations of the satellite. Callisto does not have an intrinsic magnetic field (Khurana *et al.* 1998a), an observation also consistent with the absence of a metallic core in Callisto. Callisto's surface shows no sign of internal activity (Greeley *et al.* 2000), consistent with a partially differentiated state. Callisto is not tidally heated, so this potential heat source could not have differentiated the satellite. However, Callisto may have a subsurface liquid water ocean within its ice-dominated outer layer (Khurana *et al.* 1998b, Kivelson *et al.* 1999), effectively decoupling the surface from the slow differentiation beneath.

## ACKNOWLEDGMENTS

This work was sponsored by the Galileo Project and was performed at the Jet Propulsion Laboratory, California Institute of Technology, under contract with NASA. G.S., W.B.M., and P.C.T. acknowledge support by grants from NASA through the Galileo Project at JPL and the Planetary Geology and Geophysics program.

## REFERENCES

- Anderson, J. D. 1974. Lectures on physical and technical problems posed by precision radio tracking. In *Experimental Gravitation* (B. Bertotti, Ed.), pp. 163–199. Academic Press, New York.
- Anderson, J. D., E. L. Lau, W. L. Sjogren, G. Schubert, and W. B. Moore 1996. Gravitational constraints on the internal structure of Ganymede. *Nature* **384**, 541–543.
- Anderson, J. D., E. L. Lau, W. L. Sjogren, G. Schubert, and W. B. Moore 1997. Gravitational evidence for an undifferentiated Callisto. *Nature* **387**, 264–266.
- Anderson, J. D., G. Schubert, R. A. Jacobson, E. L. Lau, W. B. Moore, and W. L. Sjogren 1998a. Europa's differentiated internal structure: Inferences from four Galileo encounters. *Science* **281**, 2019–2022.
- Anderson, J. D., G. Schubert, R. A. Jacobson, E. L. Lau, W. B. Moore, and W. L. Sjogren 1998b. Distribution of rock, metals, and ices in Callisto. *Science* **280**, 1573–1576.
- Cohen, E. R., and B. N. Taylor 1999. The fundamental physical constants. *Phys. Today* **52**, BG5–BG9.
- Davies, M. E., T. R. Colvin, M. J. S. Belton, J. Veverka, and P. Thomas 1994. The direction of the north pole and the control network of asteroid 951 Gaspra. *Icarus* **107**, 18–22.
- Davies, M. E., V. K. Abalakin, M. Bursa, J. H. Lieske, B. Morando, D. Morrison, P. K. Seidelmann, A. T. Sinclair, B. Yallop, and Y. S. Tjuffin 1996. Report of the IAU/IAG/COSPAR working group on cartographic coordinates and rotational elements of the planets and satellites: 1994. *Celes. Mech.* **53**, 127–148.
- Dermott, S. F., and P. C. Thomas 1988. The shape and internal structure of Mimas. *Icarus* **73**, 25–65.
- Dermott, S. F., and P. C. Thomas 1994. The determination of the mass and mean density of Enceladus from its observed shape. *Icarus* **109**, 241–257.
- Greenberg, R. 1982. Orbital evolution of the Galilean satellites. In *Satellites of Jupiter* (D. Morrison, Ed.), pp. 65–92. Univ. of Arizona Press, Tucson.
- Greeley, R., J. E. Klemaszewski, and R. Wagner 2000. Galileo views of the geology of Callisto. *Planet. Space Sci.* **48**, 829–853.
- Hubbard, W. B., and J. D. Anderson 1978. Possible flyby measurements of Galilean satellite interior structure. *Icarus* **33**, 336–341.
- Jacobson, R. A., R. J. Haw, T. P. McElrath, and P. G. Antreasian. A comprehensive orbit reconstruction for the Galileo Prime Mission in the J2000 system. Presented at AAS/AIAA Astrodynamics Specialist Conference, American Astronautical Society, Girdwood, Alaska, 1999.
- Kaula, W. M. 1966. *Theory of Satellite Geodesy*. Blaisdell, Waltham, MA.
- Khurana, K. K., M. G. Kivelson, C. T. Russell, R. J. Walker, and D. J. Southwood 1998a. Absence of an intrinsic magnetic field on Callisto. *Nature* **387**, 262–264.
- Khurana, K. K., M. G. Kivelson, D. J. Stevenson, G. Schubert, C. T. Russell, R. J. Walker, S. Joy, and C. Polauskey 1998b. Induced magnetic fields as evidence for subsurface oceans in Europa and Callisto. *Nature* **395**, 777–780.
- Kivelson, M. G., K. K. Khurana, D. J. Stevenson, L. Bennett, S. Joy, C. T. Russell, R. J. Walker, C. Zimmer, and C. Polauskey 1999. Europa and Callisto: Induced or intrinsic fields in a periodically varying plasma environment. *J. Geophys. Res.* **104**, 4609–4646.
- Lawson, C. L. and R. J. Hanson 1974. *Solving Least Squares Problems*. Prentice-Hall, Englewood Cliffs, N.J.
- McKinnon, W. B. 1998. Mystery of Callisto: Is it undifferentiated? *Icarus* **130**, 534–539.
- Moyer, T. D. 1971. *Mathematical formulation of the double precision orbit determination program (DPODP)*, Tech. Rep. No. TR 32-1527, Jet Propulsion Laboratory, Pasadena.
- Mueller, S., and W. B. McKinnon 1988. Three-layered models of Ganymede and Callisto: Compositions, structures, and aspects of evolution. *Icarus* **76**, 437–464.
- Schubert, G., D. Limonadi, J. D. Anderson, J. K. Campbell, and G. Giampieri 1994. Gravitational coefficients and internal structures of the Galilean satellites: An assessment of the Galileo Orbiter mission. *Icarus* **111**, 433–440.
- Tapley, B. D. 1973. Statistical orbit determination theory. In *Recent Advances in Dynamical Astronomy* (B. D. Tapley, and V. Szebehely, Eds.), pp. 396–425. Reidel, Dordrecht, Boston, MA.
- Thomas, P. C., M. E. Davies, T. R. Colvin, J. Oberst, P. Schuster, G. Neukum, M. H. Carr, A. McEwen, G. Schubert, and M. J. S. Belton 1998. The shape of Io from Galileo limb measurements. *Icarus* **135**, 175–180.
- Zharkov, V. N., V. V. Leontjev, and A. V. Kozenko 1985. Models, figures, and gravitational moments of the Galilean satellites of Jupiter and icy satellites of Saturn. *Icarus* **61**, 92–100.